Biochimica et Biophysica Acta 1837 (2014) 186–192

Contents lists available at ScienceDirect

Biochimica et Biophysica Acta

journal homepage: www.elsevier.com/locate/bbabio

Charge transfer through a cytochrome multiheme chain: Theory and simulation

Fabian Burggraf [a,b], Thorsten Koslowski [a,*]

[a] Institut für Physikalische Chemie, Universität Freiburg, Albertstraße 23a, D-79104 Freiburg im Breisgau, Germany
[b] Institut für Technische Thermodynamik, Deutsches Zentrum für Luft- und Raumfahrt (DLR), Pfaffenwaldring 38–40, D-70569 Stuttgart, Germany

ARTICLE INFO

Article history:
Received 5 June 2013
Received in revised form 22 August 2013
Accepted 10 September 2013
Available online 18 September 2013

Keywords:
Charge transfer
Photoreaction center
Molecular dynamics
Simulations
Marcus theory
Rps. viridis

ABSTRACT

We study sequential charge transfer within a chain of four heme cofactors located in the c-type cytochrome subunit of the photoreaction center of *Rhodopseudomonas viridis* from a theoretical perspective. Molecular dynamics simulations of the thermodynamic integration type are used to compute two key energies of Marcus' theory of charge transfer, the driving force ΔG and the reorganization energy λ. Due to the small exposure of the cofactors to the solvent and to charged amino acids, the outer sphere contribution to the reorganization energy almost vanishes. Interheme effective electronic couplings are estimated using ab initio wave functions and a well-parameterized semiempirical scheme for long-range interactions. From the resulting charge transfer rates, we conclude that at most the two heme molecules closest to the membrane participate in a fast recharging of the photoreaction center, whereas the remaining hemes are likely to have a different function, such as intermediate electron storage. Finally, we suggest means to verify or falsify this hypothesis.

1. Introduction

Charge transfer is a fundamental chemical reaction underlying important processes of life, such as photosynthesis, respiration or DNA damage and repair. Understanding these phenomena on a molecular level may also help to improve technical devices such as organic solar cells, sensors or functional, conducting nanostructures. Here, we focus on a model system of photosynthesis, the photoreaction center of the purple bacterium *Rps. virdis*.

In contrast to plants or cyanobacteria, purple bacteria conduct a strictly anoxygenic photosynthesis. By a series of cyclic electron transfer reactions, a reducing agent is recycled, and oxygen production is avoided. As a consequence, the photosynthetic apparatus remains comparatively simple and contains only a single photosystem, the so-called photosynthetic reaction center (PRC). Solving its structure [1] had been an outstanding contribution to understand photosynthesis, and the PRC remains an important model system to date. With the help of the structure presented in Fig. 1, we give a brief overview of the mechanism of harvesting light and converting its energy into a potential generated by the separation of two charges.

Upon irradiation, the so-called special pair of bacteriochlorophylls, P_{865} is excited with a main absorption maximum at the wave length of the index (in nm). The electron is rapidly transferred along the L branch of the protein to a bacteriophaeophytine (BPh b or bp) with the aid of an auxiliary bacteriochlorophyll b (BCl b). Subsequently, the electronic charge is transported along a pair of two quinones (Q_A, Q_B), probably assisted by the histidines coordinating an intervening iron ion [2]. Finally, the terminal molecule of the electron transfer chain, a ubiquinone (Q_B), will exit the PRC. To restart the photoreaction, the special pair cation has to be reduced by an electron localized on a charge carrier on the periplasmatic side of the protein.

In purple bacteria, the electron flow from the cytochrome bc_1 complex to the reaction center is usually mediated by the soluble electron carrier cytochrome c_2 [3]. In many species the photooxidized special pair P^+_{865} is not reduced directly by cytochrome c_2, but with the help of a multiheme cytochrome subunit, which is directly associated with the photoreaction center [4,5]. Although these multiheme cytochromes are known to act as an immediate electron donor to the special pair [6–9,22,23], the detailed mechanism of the electron transduction through the multiheme chain is still poorly understood. The structural organization of the four heme groups in the cytochrome subunit of the photoreaction center of *Rhodopseudomonas viridis* in an almost linear arrangement has become evident once the X-ray structure of the PRC was available [1], triggering the idea of a sequential downhill electron transfer process involving all four hemes. However, in its simplest version this view is not compatible with a strongly alternating midpoint potentials along the assumed charge transfer path [7,10–14,19]. Subsequent studies have shown that a fingerprint of four clearly distinguishable heme potentials can be found in many other photosynthetic bacteria [15–18]. Mutation experiments have demonstrated that charged amino acid residues in the vicinity of the heme groups have a crucial effect on their electrostatic properties and therefore make them controllable

* Corresponding author.

0005-2728/$ – see front matter
http://dx.doi.org/10.1016/j.bbabio.2013.09.005

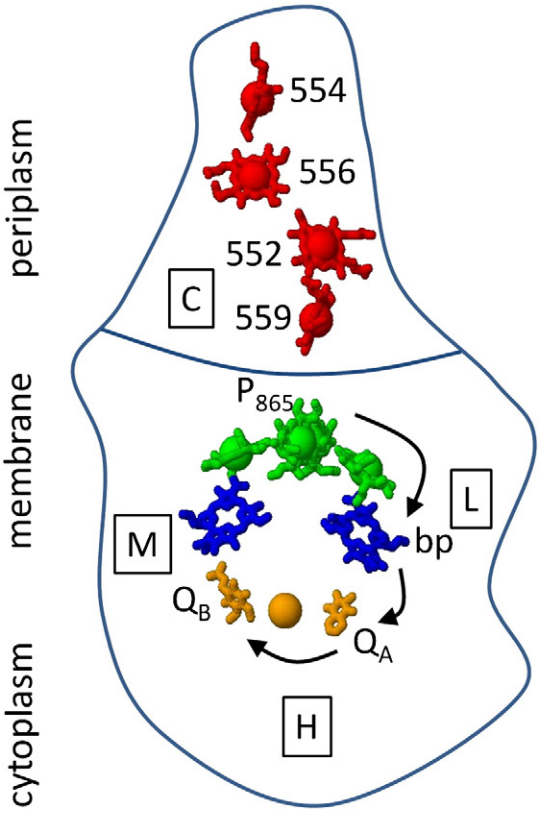

Fig. 1. Cartoon model of the heme electron transfer chain of the photosynthetic reaction center of *Rps. viridis* based on the structure of ref. [1].

to a certain extent [19,20]. Chen et al. have shown that the transfer rates of the interheme electron flow are particularly sensitive to changes in the redox potential of the hemes involved [21].

In the cytochrome subunit of the reaction center of *Rps. viridis* electrons are believed to be transferred through a linear chain of four heme groups to the special pair bacteriochlorophyll dimer P_{865}, the site of the primary photooxidation [7,11]. The midpoint potentials of the four heme groups have been determined experimentally, they are arranged in a low–high–low–high pattern starting at the periplasm side of the complex: heme-c_{554} ($E_M = -60$ mV), heme-c_{556} ($E_M =$ 320 mV), heme-c_{552} ($E_M = 20$ mV) and heme-c_{559} ($E_M = 380$ mV). Heme-c_{559} is the closest cofactor to the special pair and transfers an electron to P_{865}^{+} in 100–200 ns, depending on temperature and redox states of the heme groups [22–25]. It is well established that heme-c_{559} is the direct electron donor to the oxidized special pair [26]. The oxidized heme-c_{559} is then rereduced on a time scale of 2 μs by an electron transfer involving heme-c_{556} and heme-c_{552} [10,22,23,26]. To our knowledge, direct evidence for the functional role of heme-c_{556} is still missing. However, on the basis of kinetic studies it has been suggested that the first heme is the electron acceptor for the soluble electron donor cytochrome c_2 [27–29].

Despite extensive spectroscopic studies [10,11,23,25,30–32] the charge transfer processes within the cytochrome subunit of the photoreaction center of *Rps. viridis* have not been understood completely. Open questions include (i) the function of the four heme moieties, especially the role of the two low-potential hemes, (ii) the impact and biological function of the low–high–low–high arrangement of the heme midpoint potentials and (iii) the detailed pathway of the electron transfer through the subunit. From a theoretical perspective, Bombarda and Ullmann have addressed these questions using an electrostatic continuum model both for the protein and the solvent [33].

The remaining part of this article is organized as follows. In the following section, we will present the technical details of the molecular dynamics simulations and the associated thermodynamic integration scheme, leading to two parameters of Marcus' theory of charge transfer, the driving force and the reorganization energy. In the third section, we describe the electronic structure computations leading to the effective electronic couplings within the heme chain. In the fourth section, the results are integrated into Marcus' theory to compute charge transfer rates. The results are discussed, and conclusions are derived in the final section of the paper.

2. Molecular dynamics and thermodynamic integration

2.1. Force field parameters

While the standard force fields used in the *Amber* molecular modeling suite [34] are designed for the simulation of organic molecules and large biomolecules as proteins or nucleic acids, they are not able to describe transition metal complexes appropriately. Giammona [35] has generated force field parameters for the heme group that can be used supplementary to the *Amberff99SB* force field [36]. These parameters describe a heme group with a Fe^{2+}-ion as central atom. When simulating an interheme electron transfer reaction, a force field must also be able to describe the change of the oxidation state of the iron ion and the resulting change of the charge distribution in the ligand system.

In compounds containing late transition elements such as iron, correlation effects play an important role. They can usually not be adequately described by a Hartree–Fock electronic structure computation, which is the basis of the standard parametrization scheme of the *Amber* molecular modeling suite within the *Antechamber* routine. Hence, we took refuge to ab initio density functional theory for the computations of the missing force field parameters. Based on geometry optimizations using the OLYP functional and a 6-311G basis set, we have calculated the atomic partial charges for both the Fe^{2+} and the Fe^{3+} heme group. The resulting charge distribution is characterized by an excess charge that is not confined to the central iron atom, but is extended over a considerable fraction of the porphyrine system.

The thus computed excess atomic partial charges have been added to the *Amberff99SB* parameters and the resulting force field tested within a standard molecular dynamics simulation of the cytochrome subunit. In this simulation, a model system containing the protein backbone, all four heme cofactors and a 10 Å box of about 12,000 TIP3P water molecules has been used. The system has been subject to a 5000 steps steepest decent minimization followed by a 30 ps temperature equilibration up to 300 K in a *NVT* ensemble and a 40 ps *NPT* volume equilibration at 300 K. The molecular dynamics simulation was finally conducted in a *NPT* ensemble for 2 ns with snapshots of the protein geometry being taken each femtosecond. These structure snapshots served as a geometrical basis for the electronic structure computations described in the next section.

2.2. Thermodynamic integration

Based on the preequilibrated structure of the cytochrome subunit of the bacterial photoreaction center several model systems with different charge distributions were generated, only the four heme molecules act as potential centers of charge localization. We use a variant of the thermodynamic integration (TI) scheme [37] adapted to charge transfer processes [38,39] and refer the reader to these papers for the technical details.

In a thermodynamic integration, an additional parameter Λ is introduced into the potential energy of the system; it acts as an interpolation parameter between the potential energy of an educt and a product state. For charge transfer processes, the only difference between these potential energies lies in their charge distributions. Integrating the derivatives of the potential energies with respect to

Λ within a molecular dynamics simulations gives rise to the free enthalpy of the process,

$$\Delta G = \int_0^1 (\partial V/\partial \Lambda) d\Lambda. \quad (1)$$

The reorganization energies of the charge transfer reaction correspond to $\partial V/\partial\Lambda$ values extrapolated to $\Lambda = 0$ and $\Lambda = 1$.

We consider the reactions heme-c_{554}⇌heme-c_{556}, heme-c_{556} ⇌heme-c_{552} and heme-c_{559}⇌heme-c_{559}. With a series of these TI-transformations, all three consecutive charge transfer steps in the cytochrome subunit have been simulated. Each of these transformations has been divided into nine equidistant simulation windows with Λ values ranging from $\Lambda = 0.1$ to $\Lambda = 0.9$. Every Λ window was simulated for 200 ps in a *NPT* ensemble at $T = 300$ K and $p = 1$ bar pressure, allowing the system to adapt to the new charge distribution. Then, the $\partial V/\partial\Lambda$ values have been accumulated and averaged in a 0.5 ns production run resulting in a total simulation time of 6.3 ns for each simulation window. The resulting Λ-dependant free energy curves all show the same characteristics (Fig. 2). While the first and the last charge transfer steps through the heme cascade show negative $\partial V/\partial\Lambda$-values – resulting in negative value for the free energy – the transfer of an electron from heme-c_{556} to heme-c_{552} seems to be an endergonic process. The computation of the free enthalpy differences ΔG for the investigated charge transfer steps made use of a linear interpolation between the individual Λ-windows. Furthermore, the $\partial V/\partial\Lambda$-values for the initial ($\Lambda = 0$) and the final states ($\Lambda = 1$) were obtained by linear extrapolation. As a result, the experimentally observed rollercoaster-like arrangement of the heme midpoint potentials is reflected by the computed ΔG-values. For the forward reaction we identify the first ($554 \rightarrow 556$) and the last ($552 \rightarrow 559$) electron transfer step to be exergonic with free enthalpy differences of $\Delta G = -0.16$ eV and $\Delta G = -0.34$ eV respectively. With $\Delta G = 0.36$ eV, the electron transfer from heme-c_{556} to heme-c_{552} is considerably endergonic. This free enthalpy landscape is not affected significantly by introducing an additional charge to the heme chain [43].

For all simulation windows, the $\partial V/\partial\Lambda$-values exhibit a standard deviation of about 0.1 eV giving rise to a similar error upon integration, a more thorough data analysis including time correlation effects leads to a similar error of 80 meV (ref. [40], p.108). The question of the quality of the ΔG values can be addressed by comparing them to the differences between the experimental midpoint potentials, as listed in Table 1. The enthalpies for the second and the third reaction lie well within the statistical error, whereas the reaction enthalpy of the first reaction is considerably underestimated. Nevertheless, all ΔG values exhibit a modulus that is sufficiently large to classify the corresponding reaction as endergonic or exergonic.

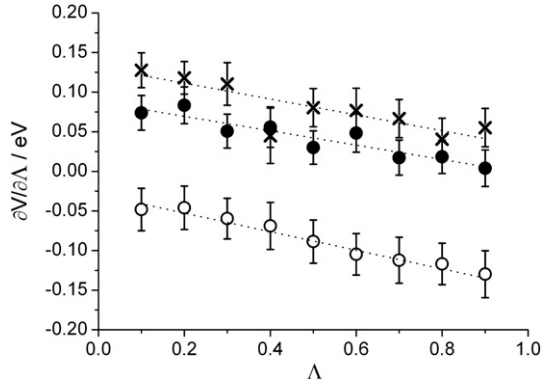

Fig. 2. Thermodynamic integration data, $\partial V/\partial\Lambda$ and their statistical errors as a function of the potential energy interpolation parameter Λ for the interheme hole charge transfer steps $552 \rightarrow 556$ (○), $556 \rightarrow 554$ (●) and $559 \rightarrow 552$ (×). All energies in electron Volts.

Table 1
Fundamental energy parameters of the interheme charge transfer reactions, thermodynamic integration (ΔG, λ_{out}) and experiment (ΔE_M) [7,10–14,19]. All energies in electron Volts (eV).

Reaction	ΔE_M	ΔG	λ_{out}
$554 \rightarrow 556$	−0.37	−0.16	0.03
$556 \rightarrow 552$	+0.29	+0.36	0.03
$552 \rightarrow 559$	−0.36	−0.34	0.09

Whereas most mixed potential functions $V(\Lambda)$ cannot be assigned to realistic physical intermediate states of the charge transfer reaction, the two starting and end points of the simulation are described by $V(\Lambda = 0)$ and $V(\Lambda = 1)$. At these points, the $\partial V/\partial\Lambda$-values reflect the energy difference when inverting the initial and the final state. Thus, they can be interpreted as the outer-sphere contributions λ_{out} to the reorganization energy in terms of Marcus' theory of charge transfer. None of the calculated outer sphere reorganization energies exceeds 0.1 eV, they vanish within the errors of 100 meV typically arising from our thermodynamic integration calculations. The results are in accord with cyclic voltammetric measurements of the reorganization energies in monoheme cytochrome-c complexes: Bortolotti et al. [41] have demonstrated that the solvent accessibility of the heme groups is correlated to the reorganization energy. In that work, the solvent accessibility of a cofactor in a protein matrix is characterized by the solvent accessible surface area with values between 50 Å^2 and 90 Å^2. In that study, the λ values decrease with an increasing screening of the heme molecule by the protein environment with an extrapolated value of $\lambda = 0.2$ eV in case of a molecule completely inaccessible by the solvent. This residual value has to be interpreted as arising from inner sphere contributions to the reorganization energies. We have not considered the inhomogeneous coordination of the heme molecules – three of the His–Fe–His and one of the His–Fe–Met type – in our approach.

3. Electronic structure

In the following, we discuss the computation of the electronic structure of the heme molecules, as relevant to the calculation of key energy parameters of the electron transfer chain, namely the effective interheme couplings, t_{eff}. We make use of frontier molecular orbital (FMO) coefficients stemming from ab initio calculations on the density functional level for isolated heme cofactors. Couplings between those atomic orbitals that contribute to the FMOs localized on different hemes are evaluated using a semiempirical scheme. The resulting Hamiltonian is supplemented by a reaction field that mimics the dielectric response of the polarizable protein and solvent environment – as computed by the thermodynamic integration scheme – and an estimate of the inner sphere reorganization energy. Its eigenvalues depend on a single, unambiguous reaction coordinate. The resulting plot resembles that typical of Marcus' theory of charge transfer, the interheme couplings can be read directly as the closest approach of the ground and the excited state energy curves. We discuss the subtleties associated with the computation of couplings between sets of degenerate FMOs and give upper limits to these quantities.

As an input to the semiempirical scheme specified below, we make use of density functional calculations on iron porphyrines as models of the heme molecules. The geometry optimizations and electronic structure computations have been performed using the Gaussian 03 program package [42], the OLYP exchange-correlation functional (generally believed to well describe magnetic properties and orbital energies [43,44]) and a variety of basis sets ranging from a minimal basis to 6-311G**. Both planar porphyrines and models containing iron coordinated by $-SCH_3$ and imidazole ligands have been considered, modeling its neighbor cysteine and histidine amino acids. The iron atom constitutes the center of a Cartesian coordinate system, and its heme nitrogen neighbors lie in the *xy*-plane. Regardless of the coordination and of the

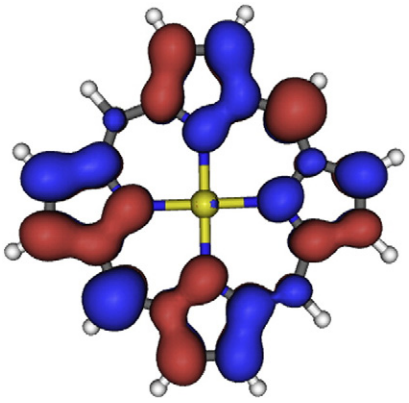

Fig. 3. Highest occupied molecular orbital (HOMO) of an iron porphyrine following the calculations outlined in Section 3. Red and blue colors correspond to positive and negative signs of the wavefunction.

basis set applied, the shape and nodal structure of the FMOs show little change. An example for a singlet state computation highest occupied molecular orbital (HOMO) is presented in Fig. 3, the lowest unoccupied molecular orbital (LUMO) is essentially related to the HOMO by a 90 degree rotation around the z axis.

The FMOs are π orbitals that exhibit a considerable delocalization and only a small contribution of iron d orbitals, an observation recurrent in the literature since early ab initio computations [45–61]. As a consequence, we have refrained from using the iron orbitals within the computation of interheme couplings. We make use of the coefficients stemming from a singlet computation as appropriate to the experimentally observed multiplicity [62–67] but have to note that computed triplet states are slightly lower in energy, as chemical intuition suggests.

In our semiempirical scheme, we denote the heme molecules as A and B and their frontier molecular orbitals as i and j. The electronic structure is described by a one-electron Hamiltonian that operates on the FMOs,

$$\hat{H} = \sum_{A,B} \sum_{i\in A} \sum_{j\in B} a_{iA}^{\dagger} a_{jB} t_{iAjB} \tag{2}$$

with creation and annihilation operators $a_{iA}^{\dagger}$ and a_{jB}. We assume that all FMOs are orthogonal, and that all interactions between orbitals located on the same site vanish. These assumptions and their impact on the intermolecular effective electronic couplings will be discussed below.

The intermolecular matrix elements can be computed as

$$t_{iAjB} = \sum_{k} \sum_{l} c_{ik} c_{jl} t_{kl}, \tag{3}$$

where the c are the expansion coefficients from a linear combination of atomic orbital (LCAO) computation on each of the molecules, and t_{kl} is an effective one-electron matrix element between atomic orbitals located on molecules A and B. The LCAO coefficients stem from a DFT calculation, again on the OLYP level. As a consequence, all intramolecular interactions are described by an ab initio scheme, whereas the intermolecular ones are treated on a semiempirical basis.

For the intermolecular couplings, we assume an exponential decay of the interactions between sets of 2p orbitals upon the interatomic distance,

$$t_{ppm}(r) = t_{ppm}^{0} exp(-\alpha r) \tag{4}$$

with $m = \sigma$ or π. For each heme, 2p π orbitals are constructed orthogonal to the plane of the molecule, and the actual interatomic matrix elements, t_{kl}, are computed as a sum of $t_{pp\sigma}$ and $t_{pp\pi}$ interactions weighted according to the Slater–Koster rules [68], thus taking the mutual orientation of the cofactors into account. The parameters of the interatomic couplings, Eq. (4), have been carefully parameterized using large basis set ab initio calculations for stacked aromatic and heterocyclic systems [69]. Nonorthogonality of the atomic orbitals is absorbed in the parameters. Their numerical values amount to $t_{pp\sigma}^{0} = 43.2$ eV, $t_{pp\pi}^{0} = -11.6$ eV and $\alpha = 1.37$ Å^{-1}.

Once an excess charge is introduced, bath or intramolecular degrees of freedom may couple to this charge, lowering the energy of the system and – for a sufficiently strong interaction – finally enable charge trapping via the formation of a small polaron. This interaction can be represented by a reaction field that is proportional to the square of the excess charge [70]. For a single molecule A, we have

$$\hat{H}_{ee} = -U n_A^2 = -U \sum_{i\in A} \sum_{j\in A} n_{iA} n_{jA} \tag{5}$$

with $\lambda = 2U$ relating the reorganization energy to the U parameter of the so-called attractive Hubbard model.

Introducing a mean-field approximation, each product of number operators can be written as

$$n_{iA} n_{jA} \simeq n_{iA} \langle n_{jA} \rangle + n_{jA} \langle n_{iA} \rangle - \langle n_{iA} \rangle \langle n_{jA} \rangle. \tag{6}$$

Here, the angles denote the computation of an expectation value. Combining the last two expressions, we arrive at

$$\hat{H}_{ee} \simeq -2U \langle n_A \rangle \sum_{i\in A} n_{ia}. \tag{7}$$

We note that for a pair of molecules and single excess charge $q = \langle n_A \rangle = 1 - \langle n_B \rangle$ holds. The total mean-field Hamiltonian matrix now reads

$$\mathrm{H} = \begin{pmatrix} -2Uq & -2Uq & t_{1112} & t_{1122} \\ -2Uq & -2Uq & t_{2112} & t_{2122} \\ t_{1112} & t_{2112} & -2U(1-q) & -2U(1-q) \\ t_{1122} & t_{2122} & -2U(1-q) & -2U(1-q) \end{pmatrix}. \tag{8}$$

This Hamiltonian matrix is rotationally invariant, and it exhibits particle-hole symmetry. It can be diagonalized, and its energies can be analyzed as a function of q, the amount of charge transferred between two heme molecules. We will turn to this analysis in the following section, and now briefly discuss problems arising from the presence of two degenerate FMOs residing on each of the hemes.

In an environment exhibiting a lower symmetry than the heme molecules – such as their host protein – the degeneracy of the two FMOs will be broken, and linear combinations of the FMOs will form in response even to a small external potential or an anisotropic reaction field. In addition, the protein will induce potential energy fluctuations as a function of time, a behavior typical for soft matter charge transfer systems [71]. Regrettably, our molecular dynamics simulations have been plagued by a drift of the two central cofactors within the supposed charge transfer chain, heme 552 and heme 554, that – albeit small in terms of the overall protein geometry – resulted in a considerable reduction of the coupling between these hemes, thus preventing the computation of time averages. Nevertheless, we are able to provide upper limits to the coupling resulting from a matrix of the type Eq. (8) regardless of the size of its diagonal elements using the theorem of Hadamard and Gershgorin [72], which is given by the sum of the moduli of each row of the matrix Eq. (8) for $U = 0$.

All actual potential energy curve calculations, as described below, have been performed with $U > 0$.

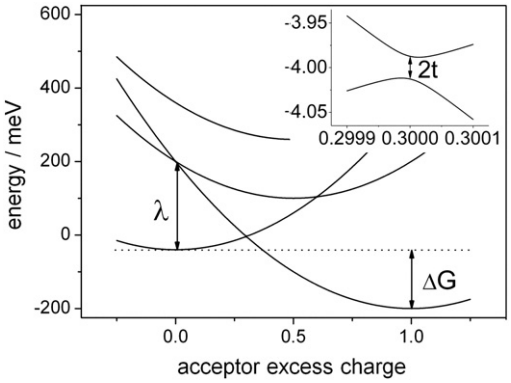

Fig. 4. Eigenvalues of the mean-field Hamiltonian matrix Eq. (8) as a function of the amount of excess charge transferred between heme 554 and 556. We set $\lambda = 0.2$ eV, use the theoretical value of $\Delta G = -0.16$ eV and find $t_{eff} = 3.5 \times 10^{-5}$ eV. All energies in electron Volts.

4. Marcus' theory and charge transfer

The eigenvalues of the Hamiltonian matrix Eq. (8) can be computed as a function of q, the amount of charge transferred, which can also be used as a convenient reaction coordinate. The resulting potential energies are displayed in Fig. 4 for $U = 0.1$ eV, corresponding to a total reorganization energy $\lambda = 2U = 0.2$ eV, as justified below.

This plot resembles the familiar Marcus picture of charge transfer, and it can be used to access the effective interheme couplings relevant to the computation of the charge transfer rate as half of the smallest energy difference between the ground state and the first excited state.

We obtain values of the order of 10^{-6} to 10^{-5} eV, with the smallest value corresponding to the charge transfer step between the two central hemes 552 and 556 that also exhibit the largest edge-to-edge distance. All numerical values are given in Table 2.

Before combining the characteristic quantities relevant to Marcus' theory of charge transfer in order to compute the rates for each step, we briefly remind ourselves of their origin: i) the driving force, ΔG, stems from a thermodynamic integration procedure, Eq. (1), based on a classical molecular dynamics simulation; ii) the outer sphere reorganization energies emerge from the same type of simulation, they correspond to $\partial V/d\Lambda$ at $\Lambda = 0$ (forward reaction, λ_f) and at $\Lambda = 1$ (backward reaction), which equal zero within the numerical accuracy of the TI procedure; iii) an inner sphere contribution, as discussed below and iv) the effective electronic coupling, t_{eff}, stemming from the analysis of plots such as Fig. 4, based on a linear combinations of molecular orbital scheme.

We make use of Marcus' expression for the nonadiabatic charge transfer rate,

$$k_{CT} = \frac{t_{eff}^2}{\hbar}\sqrt{\frac{\pi}{\lambda k_B T}}exp\left(-\frac{(\Delta G+\lambda)^2}{4\lambda k_B T}\right). \quad (9)$$

Here, λ consists of an outer sphere contribution λ_{out} – as computed within the thermodynamic integration scheme – and an inner sphere contribution λ_{in} stemming from the rearrangement of bond lengths once an excess charge is introduced.

We set the internal reorganization energy to 0.2 eV, a value compatible with an extrapolation to a zero surface accessibility by aqueous solvents, as estimated by Bortolotti et al. on the basis of their molecular dynamics simulations [41]. We note that the overall picture described in the following does not vary qualitatively for λ_{in} values that lie within a reasonable interval ranging from 0.05 to 0.5 eV.

For a given t_{eff} and λ, a maximum rate emerges at $\lambda = -\Delta G$, we refer to this quantity as k_{CT}^{max}.

For the forward reaction, we find a fast first ($554 \rightarrow 556$) and final ($552 \rightarrow 559$) charge transfer step, with $k_{CT} = 4.3 \times 10^7$ and 3.6×10^7 s^{-1}, respectively. The intermediate step, $556 \rightarrow 552$ is, however, very slow and only amounts to 5.9×10^{-3} s^{-1}, a value that is in no way compatible with the experimentally observed time scale of 2 μs. The slow charge transfer rate is both due to the strong uphill reaction enthalpy and the small interheme coupling, which can be traced back to the large edge-to-edge distance between the hemes 552 and 556. Naturally, for the backward reaction, we find a reversed kinetic scheme: comparatively fast electron transfer takes place between the hemes 552 and 556 with $k_{CT} = 1.1 \times 10^4$ s^{-1}, a similar value of 7.2×10^4 s^{-1} for charge transfer between the cofactors 556 and 554 emerges, but only a comparatively small rate of 44 s^{-1} for charge hopping between the hemes 559 and 552 can be observed.

Changing the total population on the four hemes to two electrons and two holes does not change these values significantly. Recently, we have argued that aromatic amino acids or salt bridges placed between the chromophores may play the role of stepping stones in ground state [2,73] and excited state [74] electron transfer. In the case of the *Rps. viridis* cytochrome c oxidase structure, however, we have failed to identify suitable candidates bridging the kinetic bottleneck. All reactions described here lie within or close to the inverse regime of Marcus' theory of charge transfer, where for example quantum corrections may become significant [75]. Even considering these, the interheme couplings are too small and the activation barrier is too large to induce a significant speedup close to the experimentally observed rate.

Table 2
Interheme couplings, t_{eff}, within the charge transfer chain, variational approach (VA) results and limits set by the theorem of Hadamard–Gershgorin (HG), both in electron Volts (eV). Forward, backward and maximum reaction rates k_{CT}^f rates k_{CT}^b and k_{CT}^{max} in s^{-1}.

Reaction	t_{eff}^{VA} (eV)	t_{eff}^{HG} (eV)	k_{CT}^f (s^{-1})	k_{CT}^b (s^{-1})	k_{CT}^{max} (s^{-1})
$554 \rightarrow 556$	3.5×10^{-5}	4.8×10^{-5}	4.3×10^7	7.2×10^4	4.7×10^7
$556 \rightarrow 552$	1.0×10^{-6}	1.2×10^{-6}	5.9×10^{-3}	1.1×10^4	3.8×10^4
$552 \rightarrow 559$	5.0×10^{-5}	6.9×10^{-5}	3.6×10^7	44	9.5×10^7

5. Concluding remarks

By a combination of thermodynamic integration calculations and quantum chemical computations, we have addressed the energetics and kinetics of a charge transfer within the multiheme chain of the photoreaction center of *Rps. viridis*. Concerning the statistical and systematic inaccuracies of the thermodynamic integration scheme, the reaction enthalpies, ΔG, are in good agreement with the experimentally observed differences between the heme redox potentials. We note a vanishing outer sphere reaction enthalpy, $\lambda_{out} \simeq 0$, in accord with recent molecular dynamics simulations on a broad spectrum of cytochromes [41]. The thermodynamic data and the small effective couplings between the two central hemes 556 and 552 lead to a prohibitively large time scale of seconds to minutes for recharging the photosynthetic cycle.

We are left with the conclusion that the hemes 552 and 559 may well participate in recharging the photoreaction center within microseconds, whereas the energetics and kinetics involving the cofactors 554 and 556 suggest a different role of these molecules. This may involve electron storage operative in the dark state: whenever the electron hole at the special pair is filled, a surplus electron can be slowly transferred to these hemes and stored there, so that cytochrome c_2 can be released and its overall level can be held comparatively low. In addition, in this way an unpaired electron is removed from a soluble species, thus potentially reducing the formation of free radicals in the periplasm. Of course, this view requires that cytochrome c_2 docks to the cytochrome subunit of the photoreaction center in the vicinity of the hemes 552 and 559 rather than in the proximity of heme 554. In this manner, our hypothesis can be verified by the identification of redox complexes that exhibit binding close to the membrane, whereas

binding in the vicinity of heme 554 would falsify our idea. We can only encourage X-ray crystallographers to publish structures of this complex, even if it exhibits an unconventional coordination. In this context, in silico docking studies may also be helpful. Furthermore, it may be interesting to have a look at the molecular evolution of the purple bacteria photoreaction center: our hypothesis suggests that one or two hemes are essential to the functionality of the cytochrome c subunit and are introduced early, whereas the presence of additional hemes is useful, but not necessary, which suggests a later appearance on the phylogenetic tree.

We have to note that using a dielectric continuum approach to both the protein and the solvent and the empirical Dutton–Moser dependence of the effective intermolecular electronic couplings [76], Bombarda and Ullmann have come to different numerical results and a different interpretation of charge transfer in the cytochrome c subunit of the same organism: fast recharging is possible, and its rate depends on the oxidation state of all hemes and the special pair. From our point of view, this striking difference can be mainly attributed to the following phenomenon. From our experience [73,77] the Dutton–Moser rule seriously overestimates long-range effective electronic couplings in the absence of charge transfer stepping stones or low-energy superexchange partners, leading to a much faster charge transfer rate.

In simulations of simple systems exhibiting charge transfer, such as the paradigmatic Ru(II)/Ru(III) pair, the use of polarizable water models has resulted in the reduction of outer sphere reorganization energies by up to 22% [78]. Whereas the use of force fields of this type is generally advisable, it is not likely to affect the main result of our work concerning reorganization, namely a vanishing outer sphere reorganization energy. Currently, we are restricted to nonpolarizable water models such as TIP3P due to the sheer size of the systems and the long simulation times required to achieve proper statistics.

Acknowledgements

It is a pleasure to thank Holger Dau, Thorsten Friedrich and Matthias Ullmann for fruitful discussions and helpful comments. Financial support by the Deutsche Forschungsgemeinschaft (DFG) via the grant Ko 1384/12-1 is gratefully acknowledged.

References

[1] J. Deisenhofer, O. Epp, K. Miki, R. Huber, H. Michel, Structure of the protein subunits in the photosynthetic reaction center of *Rhodopseudomonas viridis* at 3 Å resolution, Nature 318 (1985) 618–624.
[2] F. Burggraf, T. Koslowski, The simulation of interquinone charge transfer in a bacterial photoreaction center highlights the central role of a hydrogen-bonded non-heme iron complex, BBA 1807 (2011) 53.
[3] P.M. Wood, Do photosynthetic bacteria contain cytochrome c_1? J. Biochem. 189 (1980) 385–391.
[4] T. Kihara, B. Chance, Cytochrome photooxidation at liquid nitrogen temperatures in photosynthetic bacteria, Biochim. Biophys. Acta 189 (1969) 116–124.
[5] D.A. Shill, P.M. Wood, A role for cytochrome c_2 in *Rhodopseudomonas viridis*, Biochim. Biophys. Acta 764 (1984) 1–7.
[6] D. DeVault, B. Chance, Studies of photosynthesis using a pulsed laser. I. Temperature dependence of cytochrome oxidation rate in chromatium. Evidence for tunneling, Biophys. J. 6 (1966) 825–847.
[7] S.M. Dracheva, L.A. Drachev, A.A. Konstantinov, A.Y. Semenovu, V.P. Skulachev, A.M. Arutjunjan, V.A. Shuvalov, S.M. Zaberezhnaya, Electrogenic steps in the redox reactions catalyzed by photosynthetic reaction-centre complex from *Rhodopseudomonas viridis*, Eur. J. Biochem. 171 (1988) 253–264.
[8] A. Fukushima, K. Matsuura, K. Shimada, T. Satoh, Reaction center-B870 protein pigment complexes with bound cytochrome c-555 and c-551 from *Rhodocyclus gelatinosus*, Biochim. Biophys. Acta 933 (1988) 399–405.
[9] D.B. Knaff, A. Willie, J.E. Long, A. Kriauciunas, B. Durham, F. Millett, Reaction of cytochrome c_2 with photosynthetic reaction centers from *Rhodopseudomonas viridis*, Biochemistry 30 (1991) 1303–1310.
[10] R.J. Shopes, L.M.A. Levine, D. Holten, C.A. Wraight, Kinetics of oxidation of the bound cytochromes in reaction centers from *Rhodopseudomonas viridis*, Photosynth. Res. 12 (1987) 165–180.
[11] W. Nitschke, A.W. Rutherford, Tetraheme cytochrome c subunit of *Rhodopseudomonas viridis* characterized by EPR, Biochemistry 28 (1989) 3161–3168.
[12] A. Vermeglio, P. Richaud, J. Breton, Orientation and assignment of the four cytochrome hemes in *Rhodopseudomonas viridis* reaction centers, FEBS Lett. 243 (1989) 259–263.
[13] G. Fritzsch, S. Buchanan, H. Michel, Assignment of cytochrome hemes in crystallized reaction centers from *Rhodopseudomonas viridis*, Biochemistry 977 (1989) 157–162.
[14] G. Alegria, P.L. Dutton, Langmuir–Blodgett monolayer films of bacterial photosynthetic membranes and isolated reaction centers: preparation, spectrophotometric and electrochemical characterization, Biochim. Biophys. Acta 1057 (1991) 239–272.
[15] J.P. Allen, G. Feher, T.O. Yeates, i D.C. Rees, J. Deisenhofer, H. Michel, R. Huber, Structural homology of reaction centers from *Rhodopseudomonas sphaeroides* and *Rhodopseudomonas viridis* as determined by X-ray diffraction, Proc. Natl. Acad. Sci. 83 (1986) 8589–8593.
[16] W. Nitschke, I. Agalidis, A.W. Rutherford, The reaction-centre associated cytochrome subunit of the purple bacterium *Rhodocyclus gelatinosus*, Biochim. Biophys. Acta 1100 (1992) 49–57.
[17] W. Nitschke, M. Jubault-Bregler, A.W. Rutherford, The reaction center associated tetraheme cytochrome subunit from *Chromatium vinosum* revisited: a reexamination of its EPR properties, Biochemistry 32 (1993) 8871–8879.
[18] W. Nitschke, S.M. Dracheva, Anoxygenic Photosynthetic Bacteria, Kluwer Academic Publisher, Dodrecht, The Netherlands, 1995.
[19] M.R. Gunner, B. Honig, Electrostatic control of midpoint potentials in the cytochrome subunit of the *Rhodopseudomonas viridis* reaction center, Proc. Natl. Acad. Sci. 88 (1991) 9151–9155.
[20] P. Voigt, E.W. Knapp, Tuning heme redox potentials in the cytochrome c subunit of photosynthetic reaction centers, J. Biol. Chem. 278 (2003) 51993–52001.
[21] I.P. Chen, P. Mathis, J. Koepke, H. Michel, Uphill electron transfer in the tetraheme cytochrome subunit of the *Rhodopseudomonas viridis* photosynthetic reaction center: evidence from site-directed mutagenesis, Biochemistry 29 (2000) 3592–3602.
[22] J.M. Ortega, P. Mathis, Effect of temperature on the kinetics of electron transfer from the tetraheme cytochrome to the primary donor in *Rhodopseudomonas viridis*, FEBS Lett. 301 (1992) 45–48.
[23] J.M. Ortega, P. Mathis, Electron transfer from the tetraheme cytochrome to the special pair in isolated reaction centers of *Rhodopseudomonas viridis*, Biochemistry 32 (1993) 1141–1151.
[24] B. Dohse, P. Mathis, J. Wachtveitl, E. Laussermair, S. Iwata, H. Michel, D. Oesterhalt, Electron transfer from the tetraheme cytochrome to the special pair ion the *Rhodopseudomonas viridis* reaction center: effect of mutations of tyrosine L162, Biochemistry 34 (1995) 11335–11343.
[25] F. Rappaport, D. Bal, A. Vermglio, P. Joliot, Time-resolved electron transfer at the donor side of *Rhodopseudomonas viridis* photosynthetic reaction centers in whole cells, Photosynth. Res. 55 (1998) 317–323.
[26] S.M. Dracheva, L.A. Drachev, S.M. Zaberezhnaya, A.A. Konstantinov, A.Y. Semenov, V.P. Skulachev, FEBS Lett. 205 (1986) 41–46.
[27] E.B. Knaff, The cytochrome bc_1 complexes of photosynthetic purple bacteria, Photosynth. Res. 35 (1993) 117–133.
[28] A. Osyczka, K.V.P. Nagashima, S. Sogabe, K. Miki, M. Yoshida, K. Shimada, K. Matsuura, Interaction site for soluble cytochromes on the tetraheme cytochrome subunit bound to the bacterial reaction center mapped by site-directed mutagenesis, Biochemistry 37 (1998) 11731–11744.
[29] J.M. Ortega, F. Drepper, P. Mathis, Electron transfer between cytochrome c2 and the tetraheme cytochrome c in *Rhodopseudomonas viridis*, Photosynth. Res. 59 (1999) 147–157.
[30] M. Bixon, J. Jortner, Cytochrome oxidation in bacterial photosynthesis, Photosynth. Res. 22 (1989) 29–37.
[31] E. Nabedryk, C. Berthomieu, A. Vermglio, J. Breton, Photooxidation of high-potential (c_{559}, c_{556}) and low-potential (c_{552}) hemes in the cytochrome subunit of *Rhodopseudomonas viridis* reaction center: characterization by FTIR spectroscopy, FEBS Lett. 293 (1991) 53–58.
[32] V.P. Shinkarev, A.L. Drachev, S.M. Dracheva, The thermodynamic characteristic of four-heme cytochrome c in *Rhodopseudomonas viridis* reaction centers, as derived from a quantitative analysis of the differential absorption spectra in α-domain, FEBS Lett. 261 (1990) 11–13.
[33] E. Bombarda, G.M. Ullmann, Continuum electrostatic investigations of charge transfer processes in biological molecules using a microstate description, Faraday Discuss. 148 (2011) 173–179.
[34] D.A. Case, T.A. Darden, T.E. Cheatham, C.L. Simmerling, J. Wang, R.E. Duke, R. Luo, R.C. Walker, W. Zhang, K.M. Merz, B. Roberts, S. Hayik, A. Roitberg, G. Seabra, J. Swails, A.W. Goetz, I. Kolossvai, K.F. Wong, F. Paesani, J. Vanicek, R.M. Wolf, J. Liu, X. Wu, S.R. Brozell, T. Steinbrecher, H. Gohlke, Q. Cai, X. Ye, J. Wang, M.-J. Hsieh, G. Cui, D.R. Roe, D.H. Mathews, M.G. Seetin, R. Salomon-Ferrer, C. Sagui, V. Babin, T. Luchko, S. Gusarov, A. Kovalenko, P.A. Kollman, Amber 12 Molecular Modelling Suite, University of California, San Francisco, 2012.
[35] D.A. Giammona, An Examination of Conformational Flexibility in Porphyrins and Bulky-ligand Binding in Myoglobin, (PhD thesis) University of California, Davis, 1984.
[36] V. Hornak, R. Abel, A. Okur, B. Strockbine, A. Roitberg, Comparison of multiple amber force fields and development of improved protein backbone parameters, Proteins 65 (2006) 712–725.
[37] J. Kirkwood, J. Chem. Phys. 3 (1935) 300–313.
[38] S. Krapf, T. Koslowski, T. Steinbrecher, The thermodynamics of charge transfer in DNA photolyase — using thermodynamic integration calculations to analyze the kinetics of electron transfer reactions, Phys. Chem. Chem. Phys. 12 (2010) 9516.
[39] S. Krapf, S. Weber, T. Koslowski, The road not taken: a theoretical view of an unexpected cryptochrome electron transfer path, Phys. Chem. Chem. Phys. 14 (2012) 11518.
[40] F. Burggraf, Beiträge zur Theorie des Elektronentransfers in photosynthetischen Reaktionszentren von Purpurbakterien, (Dr. rer. nat. thesis) , 2012. 123–124 (Freiburg, also available online as http://www.freidok.uni-freiburg.de/volltexte/8802/).
[41] C.A. Bortolotti, M.E. Siwko, E. Castellini, A. Ranieri, M. Sola, S. Corni, The reorganization energy in cytochrome c is controlled by the accessibility of the heme to the solvent, J. Phys. Chem. Lett. 2 (2011) 1761–1765.

[42] M.J. Frisch, G.W. Trucks, H.B. Schlegel, G.E. Scuseria, M.A. Robb, J.R. Cheeseman, J.A. Montgomery Jr., T. Vreven, K.N. Kudin, J.C. Burant, J.M. Millam, S.S. Iyengar, J. Tomasi, V. Barone, B. Mennucci, M. Cossi, G. Scalmani, N. Rega, G.A. Petersson, H. Nakatsuji, M. Hada, M. Ehara, K. Toyota, R. Fukuda, J. Hasegawa, M. Ishida, T. Nakajima, Y. Honda, O. Kitao, H. Nakai, M. Klene, X. Li, J.E. Knox, H.P. Hratchian, J.B. Cross, V. Bakken, C. Adamo, J. Jaramillo, R. Gomperts, R.E. Stratmann, O. Yazyev, A.J. Austin, R. Cammi, C. Pomelli, J.W. Ochterski, P.Y. Ayala, K. Morokuma, G.A. Voth, P. Salvador, J.J. Dannenberg, V.G. Zakrzewski, S. Dapprich, A.D. Daniels, M.C. Strain, O. Farkas, D.K. Malick, A.D. Rabuck, K. Raghavachari, J.B. Foresman, J.V. Ortiz, Q. Cui, A.G. Baboul, S. Clifford, J. Cioslowski, B.B. Stefanov, G. Liu, A. Liashenko, P. Piskorz, I. Komaromi, R.L. Martin, D.J. Fox, T. Keith, M.A. Al-Laham, C.Y. Peng, A. Nanayakkara, M. Challacombe, P.M.W. Gill, B. Johnson, W. Chen, M.W. Wong, C. Gonzalez, J.A. Pople, Gaussian 03, Revision C.02, Gaussian, Inc., Wallingford CT, 2004.
[43] L.M. Lawson Daku, A. Vargas, A. Hauser, A. Fouqueau, M.E. Casida, Assessment of density functionals for the high-spin/low-spin energy difference in the low-spin Iron(II) Tris(2,2′-bipyridine) complex, ChemPhysChem 6 (2005) 1393.
[44] G. Ganzenmller, N. Berkaine, A. Fouqueau, M.E. Casida, M. Reiher, Comparison of density functionals for differences between the high (^5T–$2g$) and low ($^1Ai_{1g}$) spin states of Iron(II) coordination compounds: IV. Results for the ferrous complexes [Fe(L)(′NHS4′)], J. Chem. Phys. 122 (2005) 234321.
[45] N. Matsuzawa, M. Ata, D.A. Dixon, Density functional theory prediction of the second-order hyperpolarizability of metalloporphines, J. Phys. Chem. 99 (1995) 7698–7706.
[46] C. Rovira, K. Kunc, J. Hutter, P. Ballone, M. Parrinello, Equilibrium geometries and electronic structure of iron-porphyrin complexes: a density functional study, J. Phys. Chem. A 101 (1997) 8914–8925.
[47] P.M. Kozlowski, T.G. Spiro, A. Berces, Z. Zgierski, Low-lying spin states of Iron(II) porphine, J. Phys. Chem. B 102 (1998) 2603–2608.
[48] M.-S. Liao, S. Scheiner, Electronic structure and bonding in metal porphyrins, metal Fe, Co, Ni, Cu, Zn, J. Chem. Phys. 117 (2002) 205–219.
[49] D.M.A. Smith, M. Dupuis, T.P. Straatsma, Multiplet splittings and other properties from density functional theory: an assessment in iron-porphyrin systems, Mol. Phys. 103 (2005) 273–278.
[50] D.M.A. Smith, M. Dupuis, E.R. Vorpagel, T.P. Straatsma, Characterization of electronic structure and properties of a Bis(histidine) heme model complex, J. Am. Chem. Soc. 125 (2003) 2711–2717.
[51] D.M.A. Smith, M. Dupuis, T.P. Straatsma, Multiplet splittings and other properties from density functional theory: an assessment in iron–porphyrin systems, Mol. Phys. 103 (2004) 273–278.
[52] A.R. Groenhof, M. Swart, A.W. Ehlers, K. Lammertsma, Electronic ground states of iron porphyrin and of the first species in the catalytic reaction cycle of cytochrome P450s, J. Phys. Chem. A 109 (2005) 3411–3417.
[53] A. Kumar, P.C. Mishra, C.S. Verma, V. Renugopalakrishnan, Density functional study of the heme moiety of cytochrome c, Int. J. Quantum Chem. 102 (2005) 1002–1009.
[54] M.-S. Liao, J.D. Watts, M.-J. Huang, Assessment of the performance of density-functional methods for calculations on iron porphyrins and related compounds, J. Comput. Chem. 27 (2006) 1577–1592.
[55] H. Kashiwagi, S. Obara, Ab initio molecular orbital calculation of Fe-porphine with a double zeta basis set, Int. J. Quantum Chem. 20 (1981) 843–859.
[56] A. Dedieu, M.-M. Rohmer, A. Veillard, Ab initio calculations of metalloporphyrins, Adv. Quantum Chem. 16 (1982) 43–95.
[57] M.-M. Rohmer, Electronic ground state of iron(II)porphyrin. Ab initio SCF and CI calculations and computed electron deformation densities, Chem. Phys. Lett. 116 (1985) 44–49.
[58] D.C. Rawlings, M. Gouterman, E.R. Davidson, D. Feller, Theoretical investigations of the electronic states of porphyrins. III. Low-lying electronic states of porphinatoiron(II), Int. J. Quantum Chem. 28 (1985) 773–796.
[59] Y.-K. Choe, T. Nakajima, K. Hirao, Theoretical study of the electronic ground state of iron (II)porphine (II), J. Chem. Phys. 111 (1999) 3837–3845.
[60] M. Reiher, O. Salomon, A. Hess, Reparameterization of hybrid functionals based on energy differences of states of different multiplicity, Theor. Chem. Acc. 107 (2001) 48–55.
[61] K. Pierloot, The CASPT2 method in inorganic electronic spectroscopy: from ionic transition metal to covalent actinide complexes, Mol. Phys. 101 (2003) 2083–2094.
[62] G. Lang, K. Spartalian, C.A. Reed, J.P. Collman, Mössbauer effect study of the magnetic properties of S = 1 ferrous tetraphenylporphyrin, J. Chem. Phys. 69 (1978) 5424–5427.
[63] P.D.W. Boyd, A.D. Buckingham, R.F. McMecking, S. Mitra, Paramagnetic anisotropy, average magnetic susceptibility, and electronic structure of intermediate-spin S = 1 (5,10,15,20-tetraphenylporphyrin)iron(II), Inorg. Chem. 18 (1979) 3585–3591.
[64] J. Mispelter, M. Momenteau, J.M. Lhoste, Proton magnetic resonance characterization of the intermediate (S = 1) spin state of ferrous porphyrins, J. Chem. Phys. 72 (1980) 1003–1012.
[65] P. Cocolios, K.M. Kadish, Characterization of several metalloporphyrins in unusual oxidation states. The effect of axial and equatorial ligands, Isr. J. Chem. 25 (1985) 138–145.
[66] F.A. Walker, Magnetic spectroscopic (EPR, ESEEM, Mössbauer, MCD and NMR) studies of low-spin ferriheme centers and their corresponding heme proteins, Coord. Chem. Rev. 185–186 (1999) 471–534.
[67] A. Walker, Models of the bis-histidine-ligated electron-transferring cytochromes. Comparative geometric and electronic structure of low-spin ferro- and ferrihemes, Chem. Rev. 104 (2004) 589–615.
[68] J.C. Slater, G.F. Koster, Simplified LCAO method for the periodic potential problem, Phys. Rev. 94 (1954) 1498–1524.
[69] T. Cramer, S. Krapf, T. Koslowski, DNA charge transfer: an atomistic model, J. Phys. Chem. B 108 (2004) 11812;
T. Cramer, Ladungstransfer in DNA: Ein atomistisches Modell, University of Freiburg, 2006. 46–49 (Dr. rer. nat. thesis, Available online as http://www.freidok.uni-freiburg.de/volltexte/2592/).
[70] N. Utz, T. Koslowski, Variational approach to charge transfer reactions in bridged triarylamines, Chem. Phys. 282 (2002) 389.
[71] T. Cramer, T. Steinbrecher, A. Labahn, T. Koslowski, Electronic and dynamic aspects of DNA charge transfer, Phys. Chem. Chem. Phys. 7 (2005) 4039.
[72] K. Mathiak, P. Stingl, Grupppentheorie, Vieweg, Braunschweig, 1967. 137–138.
[73] C. Wittekindt, M. Schwarz, T. Friedrich, T. Koslowski, Aromatic amino acids as stepping stones in charge transfer in respiratory complex I: an unusual mechanism deduced from atomistic theory and bioinformatics, JACS 131 (2009) 8134.
[74] T. Biskup, K. Hitomi, E.D. Getzoff, S. Krapf, T. Koslowski, E. Schleicher, S. Weber, Unexpexted electron transfer in cryptochrome identified by time-resolved EPR spectroscopy, Angew. Chem. Int. Ed. 50 (2011) 12647.
[75] P. Siders, R.A. Marcus, Quantum effects for electron-transfer reactions in the inverted region, JACS 103 (1981) 748.
[76] C.C. Moser, J.M. Keske, K. Warncke, R.S. Farid, P.L. Dutton, Nature 355 (1992) 796–802; C.C. Page, C.C. Moser, X. Chen, P.L. Dutton, Nature 402 (1999) 47–52.
[77] T. Koslowski, F. Burggraf, S. Krapf, T. Steinbrecher, C. Wittekindt, Recent progress in biological charge transfer theory and simulation, Biochim. Biophys. Acta Bioenerg. 1817 (2012) 1955.
[78] J. Blumberger, G. Lamoureux, Reorganization free energies and quantum corrections for a model electron self-exchange reaction: comparison of polarizable and non-polarizable solvent models, Mol. Phys. 106 (2008) 1597–1611.